Human Airway Smooth Muscle Cell Orientation and Phenotype are altered when cultured on Aligned Electrospun Scaffolds

G.E.Morris[1], J.C. Bridge[1], O. M. I. Eltboli[2], M. P. Lewis[6], A.J. Knox[2], J.W. Aylott[3], C.E. Brightling[4] A.M. Ghaemmaghami[5], F.R.A.J. Rose[1]

1 Division of Drug Delivery and Tissue Engineering, Centre for Biomolecular Sciences, School of Pharmacy, University of Nottingham, UK.

2 Division of Respiratory Medicine, School of Clinical Sciences, University of Nottingham, UK.

3 Laboratory of Biophysics and Surface Analysis, School of Pharmacy, University of Nottingham, UK.

4 NIHR Respiratory Biomedical Research Unit, University of Leicester, UK.

5. Division of Immunology and Allergy, School of Molecular Medical Sciences, University of Nottingham, UK.

6. 6Musculoskeletal Biology Research Group, School of Sport Exercise and Health Sciences, Loughborough University, Loughborough, United Kingdom

Running Head:

Airway Smooth Muscle Altered Phenotype on Aligned Fibres (57 characters – max 60)

Corresponding Author:

Felicity RAJ Rose (BSc, PhD).

Division of Drug Delivery and Tissue Engineering,

Centre for Biomolecular Sciences,

School of Pharmacy,

University of Nottingham,

UK.

Telephone: +44(0)115 8467856

Fax: +44(0)115 951 1522

Email: felicity.rose@nottingham.ac.uk

Abstract

Human airway smooth muscle (HASM) contraction plays a central role regulating airway resistance in both healthy and asthmatic bronchioles. *In vitro* studies that investigate the intricate mechanisms that regulate this contractile process are predominantly conducted on tissue culture plastic, a rigid, 2D geometry, unlike the 3D microenvironment smooth muscle cells are exposed to *in situ*. It is increasingly apparent that cellular characteristics and responses are altered between cells cultured on 2D substrates compared to 3D topographies. Electrospinning is an attractive method to produce 3D topographies for cell culturing as the fibres produced have dimensions within the nanometre range, similar to cells' natural environment. We have developed an electrospun scaffold using the non-degradable, non-toxic, polymer polyethylene terephthalate (PET) composed of uni-axially orientated nanofibres, and have evaluated this topography's effect on HASM cell adhesion, alignment, and morphology. The fibres orientation provided contact guidance enabling the formation of fully aligned sheets of smooth muscle. Moreover, smooth muscle cells cultured on the scaffold present an elongated cell phenotype with altered contractile protein levels and distribution. HASM cells cultured on this scaffold responded to the bronchoconstrictor bradykinin. The platform presented provides a novel *in vitro* model that promotes airway smooth muscle cell development towards a more *in vivo*-like phenotype whilst providing topological cues to ensure full cell alignment.

(213 words – 250 max)

Keywords:

Airway Smooth Muscle, Tissue Engineering, Aligned fibres, Electrospinning, *In vitro* Model

Introduction

Within the airway bronchiole, human airway smooth muscle (HASM) exists as an aligned population within bundles that wrap around the bronchiole in a helical fashion (25). Smooth muscle is the key effector cell regulating airway tone, with the smooth muscle contractile state directly controlling the luminal capacity of the bronchiole. Dysfunction to the regulation of smooth muscle contraction can alter the airway tone causing both airway hyper-responsiveness (10, 44), and airway remodelling; increased smooth muscle mass is evident in both mild and severe asthmatic airways (7, 18, 30). To uncover the mechanisms controlling these physiological and pathophysiological roles attributed to HASM cells, researchers have developed numerous experimental techniques including *in vivo*, *ex vivo*, and *in vitro* platforms. The relative advantages and disadvantages in utilizing these models have been discussed extensively elsewhere (3, 5, 50).

The *in vitro* culturing of primary HASM cells has provided better understanding into the direct effects of bronchoconstrictors and inflammatory agonists on smooth muscle responses. One such technique is the real-time imaging of intracellular signalling molecules that are mobilised when muscle contraction is initiated, such as the increase in intracellular calcium concentration ($[Ca^{2+}]_i$). Many important bronchoconstrictors mediate their effects through G Protein-coupled receptors (GPCRs) that cause downstream activation of phospholipase C (PLC), leading to the generation of the second messengers inositol 1,4,5-triphosphate (IP_3) and diacylglycerol (DAG), and a subsequent increase in $[Ca^{2+}]_i$ from intracellular sarcoplasmic reticulum stores and/or Ca^{2+} influx through voltage-dependent L-type Ca^{2+} channels in the plasma membrane (4, 5). Bradykinin (BK) is a powerful bronchoconstrictor whose effects are mediated through $G\alpha_{q/11}$-coupled receptors present on HASM cells (21), which show an increase in $[Ca^{2+}]_i$ upon stimulation (31). These, and most *in vitro* studies, have been conducted on glass, or tissue culture plastic (TCP); both 2D, rigid surfaces

routinely used for cell culture. It is increasingly apparent that cell culture in a 3D, elastic, environment can greatly alter cell phenotype and cell response to their immediate surroundings (13, 14, 52).

Within a lung context, collagen gels can provide a simple 3D matrix for HASM cell culture (8, 32, 46), with cells residing in random planes of the gel-matrix opposed to an aligned population of smooth muscle cells. Advancements in tissue engineering have provided new fabrication techniques offering precise control of a substrate's nanoscale topography (29). Model studies have shown multiple cell types can be aligned over extended areas using different topological references such as plasma/extracellular matrix deposition (38), nanoimprinting (12, 26, 54), or aligned electrospun fibres (11, 51). Electrospinning produces fibrous, porous, 3D mats that closely resemble the natural extracellular matrix: The desired polymer is dissolved in an appropriate solvent and this solution is passed through a syringe with an electrical charge applied to the needle tip, causing the electrically charged solution to become attracted to a differently charged collector plate. As the polymer jet passes through the air, the solvent evaporates depositing a continuous, non-woven mesh of fibres on the collector plate. Alterations to intrinsic parameters including (but not exhaustive) polymer concentration, electrical field strength, or collector plate aspects, allow precise control over scaffold characteristics including shape, porosity, tensile strength, and fibre diameter (16, 43, 47). Electrospun fibres can be manipulated to form uni-axially-aligned scaffolds through alterations to fibre collection methods such as employing a rotating collector, or parallel electrodes (47). This technology has been applied in culturing cells requiring directional growth in oriented tissues such as neurons (9, 37, 41, 53), ligaments (42), and smooth muscle (2, 19, 51), and has recently been shown to influence stem cell differentiation (40).

In the present study we investigated the influence of fibre alignment and diameter on HASM cell characteristics using the non-degradable, non-toxic, polymer polyethylene terephthalate

(PET). Whilst randomly aligned PET fibres have been employed for the culture of aortic smooth muscle (34), and other polymers have been electrospun into aligned scaffolds for the culture of vascular (51), and bladder (2) smooth muscle, to our knowledge this is the first time HASM has been cultured on aligned electrospun fibres. The effect of this 3D aligned topography on HASM cell orientation, morphology and contractile characteristics were investigated and compared to HASM cells cultured on rigid 2D surfaces or within *in situ* airway tissue.

Materials and Methods

Materials

All materials were purchased from Sigma-Aldrich (Dorset, UK) unless stated otherwise. The Novex protein separation kit, nitrocellulose membrane, alamarBlue® solution, Fluo-4-AM, anti-mouse and anti-rabbit fluorescein isothiocyanate-conjugated (FITC) and rhodamine-conjugated secondary antibodies, and the nuclear stain Hoechst were all obtained from Invitrogen Life Technologies (Paisley, UK). Rabbit polyclonal antibodies raised against Calponin and SM22α were purchased from AbCam (Cambridge, UK). The Protease Inhibitor Cocktail Set III was purchased from Merk Millipore (Nottingham, UK)

Scaffold Fabrication

Electrospinning procedures were conducted at room temperature within in a vented chemical fume hood. PET scaffolds were produced by dissolving PET (food grade drinking bottles) in a 1:1 trifluoroacetic acid (TFA):di-chloromethane (DCM) (Fisher Chemicals, Loughborough, UK) solution to create a 10% *(w/v)* or a 20% *(w/v)* PET polymer solution. The PET polymer solution was loaded into a syringe attached to a blunt 18-gauge (G) needle (BD Falcon™, Oxford, UK) and placed in a syringe pump-driver (Harvard Apparatus Ltd., Kent, UK) set to a solution feed rate of 0.5 ml/hr or 1.5 ml/hr for the 10% or 20% scaffolds respectively. A 14 kV voltage charge was applied to the needle tip with fibres being collected on a stainless steel

grounded cylindrical mandrel positioned 15 cm from the needle tip. The mandrel was rotated at 2000 revolutions per minute (equivalent to 600 metres/minute (m/min)) to establish fibre alignment. Individual electrospinning parameters are summarized in Table 1.

Scaffold Characterization

Each scaffold-type was electrospun independently three times. Scaffolds were punctured and mounted on carbon discs prior to coating with a thin layer of gold (Balzers Union SCD 030, Balzers Union Ltd., Liechtenstein) and imaged on a scanning electron microscope (JEOL JMS-6060 LV, JEOL Ltd., Welwyn Garden City, Hertfordshire, UK). The fibre diameters and fibre orientation within the scaffolds were determined through image analysis from two samples taken from each scaffold. Four scanning electron microscope images were taken of each sample, and twenty fibre measurements were analysed from each individual image (480 fibre measurements per scaffold-type):

Fibre diameter measurements were calculated using the software package measureIT 5.1 (Olympus Soft Imaging solutions, Münster, Germany). To determine the degree of angle uniformity within the scaffolds, the mean fibre angle of an individual scaffold was determined using ImageJ, with the individual fibre deviation from this mean angle calculated.

Scaffold thickness was measured using a digital thickness gauge (accurate to 10 µm) (Mitutoyo, Coventry, UK). Scaffold mass was calculated using a top-pan balance (accurate to 0.1 mg) (Mettler Toledo, Leicester UK). The mass and scaffold thickness determined the apparent density of the scaffold and the porosity calculated as: Porosity (%) = 1-(*ad*/*bd*) x100 where *ad* is the scaffold's apparent density and *bd* is the density of pure amorphous PET (1.38 g/cm^3). Scaffold porosity was calculated using 8 mm diameter scaffold samples.

Uni-axial tensile tests were performed on three samples from three independently electrospun scaffolds (n=9). Samples (30 mm length, 3 mm width) were loaded with fibres running parallel to the applied load direction on a 5969 Universal testing system (Instron,

High Wycombe, UK), with a 50N load cell operating with an extension rate of 5 mm/min^{-1}. The Young's moduli of the samples were calculated from the resultant stress/strain curves generated using an imetrum VideoGauge.

Cell Culture on Aligned Scaffolds

Primary HASM cells from non-asthmatic individuals were isolated from bronchial biopsies at the Glenfield Hospital (Leicester, UK) as described previously (28). The research was approved by the Leicestershire Ethics Committee, and patients gave their written informed consent. HASM cells (passage 3–6) were grown in Dulbecco's modified Eagle medium (DMEM) supplemented with 10% (*v/v*) foetal calf serum, 2mM L-glutamine solution, 1% (*v/v*) antibiotic/antimycotic solution (10,000 units/mL penicillin G, 100 mg/mL streptomycin sulphate and 25 µg/mL amphotericin B). Prior to cell seeding, scaffolds were sterilized by UV-irradiation for 30 minutes on both scaffold surfaces (60 minutes total). Scaffolds were subsequently soaked in a 20% (*v/v*) antibiotic/antimycotic solution (200,000 units/mL penicillin G, 2000 mg/mL streptomycin sulphate and 500 µg/mL amphotericin B) overnight at 37^{o}C before washing in media prior to cell seeding.

Immunocytochemistry

Samples were fixed in 3.8% *(w/v)* paraformaldehyde (PFA) before permeabilization in a 0.5% *(v/v)* Triton X-100 PBS solution. Non-specific antibody binding was reduced by incubation in 3% *(w/v)* bovine serum albumin (BSA) solution proceeded by a 10% *(v/v)* goat serum solution incubation. Samples were incubated with primary antibody overnight at 4^{o}C. Protein expression was visualised with species-appropriate secondary antibodies and nuclei were visualised by Hoechst staining. Samples were viewed on a Leica TCS SP2 laser scanning confocal inverted microscope (Leica Microsystems Ltd, Milton Keynes, UK) with post-visualization image modification performed using Volocity® (Perkin Elmer, Cambridge, UK).

Cell elongation and height were analysed using Volocity® to determine individual cell's dimensions: XY images determined the long (*l*), and short (*s*), axes (length and width), with the elongation factor (EF) determined as: EF=(*l*/*s*)-1. XZ images were used to determine cell height (*h*) through cross sectional images. Cell alignment in relation to fibre orientation was determined using HASM cell nuclei angles from 4 or more images for each time point and using three HASM cell donors (n=3). Nuclei angle deviation from the fibre angle orientation was calculated and expressed as a percentage of cells orientated within 10^{o} incremental steps from the mean fibre angle.

Histological Staining

Airway biopsies were fixed in phenylmathylsulphonylfluoride (PMSF)/acetone solution before washing in water-free acetone. Samples were incubated in methyl benzoate followed by incubating in 5% methyl benzoate/glycol methanlacrylate (GMA) processing solution in three 2 hour incubations at 4°C. Biopsies were embedded in GMA after polymerization for 48 hours at 4°C. Samples were cut into 2 µm sections, and placed onto superfrost slides (Thermo Scientific, Surrey, UK). Samples were serially rehydrated through a descending ethanol (in water) concentration to 0% (*v/v*) ethanol before staining in Harris haematoxylin. Samples were serially dehydrated through an ascending ethanol concentration to 90% (*v/v*) ethanol before staining in eosin and further dehydration in 100% ethanol and xylene. Samples were air-dried, and mounted in DPX mountant prior to imaging.

Western Blotting

Airway tissue was freeze-snap dried in liquid nitrogen and stored at -80°C until use. 30 mg of tissue was homogenised using a manual homogenizer (Thermo Scientific) in lysis buffer (mM: 20 HEPES, 200 NaCl, 10 EDTA, 0.1% Triton X-100, and 0.5% Protease Inhibitor Set Cocktail III, pH 7.4). Homogenized tissue was agitated for 2 hours on an orbital shaker at 4°C before centrifugation (16'000xg, 20 minutes 4°C), with samples stored at -20°C until use. HASM cells cultured in 2D or 3D were cultured for 14 days prior to incubation in lysis

buffer. The Novex protein separation kit was used to measure protein content in HASM cells. Lysates (20 µg/lane) were separated by SDS-PAGE before transfer onto nitrocellulose membrane. Membranes were blocked in 5% non-fat dry milk in Tris-buffered saline containing 0.1% Tween (TBST) before incubation with primary antibody overnight at 4^{o}C. Membranes were incubated with horseradish peroxidise-conjugated secondary antibody and visualized by enhanced chemiluminescence (GE Healthcare, Buckinghamshire, UK). Images were captured on a LAS 4000 Luminescent Image Analyser (Fujifilm, Düsseldorf, Germany). Quantitative signals were derived by densitometric analysis using Advanced Image Data Analyzer (AIDA) software, with total protein content corrected to GAPDH protein levels.

Calcium Signalling

HASM cells were cultured for 10 days prior to loading with the Ca^{2+}-sensitive dye Fluo-4-AM (3 µM, 60 min). Scaffolds were transferred to an imaging unit where cells were maintained at 37°C in Krebs-Henseleit buffer (mM: 134 NaCl, 6 KCl, 1 $MgCl_2$, 1.2 KH_2PO_4, 10 glucose, 10 HEPES, 1.3 $CaCl_2$, pH 7.4). Real-time images were taken using an epifluorescence Nikon Eclipse TE200 microscope (Nikon, Tokyo, Japan) (×40 objective). Cells were excited at 488 nm and emission collected between 505 and 560 nm. Bradykinin (100 nM) was applied to cells, and the fluorescence emission was measured from regions of interest within the cells cytosol. $[Ca^{2+}]_i$ changes are displayed as the fluorescence emission relative to basal (F/F_0).

Data and Statistical Analysis

Data are presented for cells obtained from at least three individual HASM cell donors cultured on aligned scaffolds electrospun independently at least three times. Data are expressed as mean±standard error of mean (SEM). Data have been analysed (GraphPad Prism, San Diego CA) using T-test or one-way ANOVA and appropriate *post-hoc* testing as indicated.

Results

Scaffold Characteristics Manipulated through Alterations to Electrospinning Parameters and Fibre Collection Protocols.

To investigate whether HASM cell characteristics were affected when exposed to a 3D nanofibre topography or an aligned fibre topography, we electrospun a randomly aligned 10% (*w/v*) PET solution onto a collector plate (data not shown), or a 10% *(w/v)* or 20% *(w/v)* PET solution onto a rotating mandrel to produce aligned fibres with diameters in either the nanometre or micrometre range. Representative SEM images of the 10% and 20% scaffolds are shown in 1A, and 1B respectively. The 10% *(w/v)* PET solution produced fibre diameters of 0.2 (±0.002) μm, and the 20% *(w/v)* produced fibre diameters of 1.1 (±0.001) μm (±SEM) (1C). Both the 10% and 20% scaffolds had >90% fibres orientated within 10^{o} of the mean fibre angle and >50% of fibres orientated within 5^{o} of the mean fibre angle (1D). Both scaffolds had a porosity >80%, whilst the 20% aligned scaffold was both thicker than the 10% aligned scaffold (107 vs. 24 μm) and had a greater tensile strength (290 vs. 211 MPa). All the electrospinning parameters and individual scaffold properties are summarized in Table 1.

HASM cells show altered Phenotypic Characteristics when cultured on Aligned Electrospun Scaffolds

Airway bronchiole sections displaying longitudinal HASM cell populations (2A) were used to quantify *in situ* HASM cell alignment by referencing the angle of each cell's nucleus to indicate cellular direction, with >60% cells orientated within 10^{o} of the mean bundle angle (2E&F). HASM cells were also cultured on 22mm glass coverslips (2B), randomly aligned scaffold, 10% (2C) or 20% (2D) aligned scaffolds (cut to 22mm diameter dimensions). Cell

alignment was measured in three separate areas of the same sample to quantify cell alignment over extended distances. Cell alignment to the underlying fibre orientation was determined using nuclei angles to indicate cell direction at day 7 and day 14. With no topological references, cells grown on 2D glass coverslips (2B) or 3D randomly aligned scaffolds (data not shown) showed little orientation as a cell population over extended distances, although cells showed local alignment upon confluency by day 14 (5A&C). Cells showed consistent orientation along the 10% (2C), and 20% aligned scaffold (2D), with >40% cells orientated within 10^{o} of the mean fibre angle on both day 7 and 14 on either scaffold, compared with <25% cells showing alignment when cultured on glass (2E&F).

The effect of a 3D aligned topography on cellular dimensions was compared to 2D and 3D-randomly aligned surfaces by culturing HASM cells for 7 days prior to fixation and immunostaining for SM22α. Airway bronchiole sections displaying longitudinal and cross-sectional HASM cell populations were used to quantify *in situ* HASM cellular dimensions: XY images determined individual cell's long- and short-axis measurements to calculate their elongation factor, whilst XZ cross-sectional images determined cell height. Cells cultured on 2D substrates or residing within smooth muscle bundles were significantly shorter compared to cells cultured on 3D aligned scaffolds (3A, B, E&G). Cells showed an approximate doubling in elongation when cultured on a 3D aligned surface compared to 2D (3C, D&H); mainly due to a reduction in cell width opposed to an increase in cell length. Whilst cells were significantly more elongated within smooth muscle bundles compared to 2D cultured cells, there was no significant difference in elongation when compared to HASM cells cultured on aligned scaffolds (3F&H). Cells cultured on 3D randomly aligned scaffolds had a similar elongation factor to cells cultured in 2D, but showed a significant increase in cell height compared to 2D culture (data not shown). As there was no significant variation in cell characteristics between cells cultured on the 10% or 20% aligned scaffolds, the 10% scaffold was used in further investigations due to the nanofibrous nature of the scaffold.

Where cells attach to the extracellular environment, focal adhesion complexes link the cell's actin cytoskeleton to the surrounding matrix (49). To determine how the underlying topological references affected focal adhesion complex formation and spatial distribution, cells cultured on a 3D aligned topography were compared to those cultured upon a 2D surface. Post-seeding, cells were fixed after 3, 24, or 72 hours before immunostaining for the focal adhesion protein vinculin and co-stained for F-actin. On glass, HASM cell F-actin organised into clear stress fibres throughout the cells with vinculin clusters at each cell's distal ends (4A). This intra-cellular F-actin and vinculin expression was maintained at 24 (4B) and 72 hours (4C), with cells also displaying a flattened cell phenotype. Cells cultured on the aligned scaffolds showed little evidence of vinculin clusters at any of the time points (with localised staining apparent around the nuclei), and F-actin was not organised into stress-fibres throughout individual cells (4D). Vinculin staining became less apparent after 3 hours, and cells started to exhibit an elongated shape that aligned along the fibre orientation (3E&F).

Over a prolonged time period (3, 7, and 14 days), HASM cells cultured on 2D glass coverslips or aligned fibres were fixed and immunostained for the smooth muscle specific proteins SM22α (5A&B) and calponin (5C&D). Contractile protein distribution in HASM cells cultured on glass showed distinct stress-fibre organization, maintained a flat phenotype, and displayed increasing local cell alignment upon cell confluency at day 14 (5A&C). Conversely, HASM cells cultured on aligned scaffolds showed little evidence of contractile protein localization into stress fibres, whilst maintaining an elongated phenotype and aligned cell distribution at every time point (5B&D). The presence of gap-junctions were visualised by immunostaining for connexin-43 with qualitatively greater localized connexin-43 expression seen between adjacent HASM cells cultured on aligned scaffolds than cells cultured on glass (5F&E respectively).

HASM cells cultured on TCP or aligned scaffolds were lysed, and protein levels semi-quantitatively compared after protein levels were normalised to levels of GAPDH protein expression (6A). Cumulative data (6B) found levels of the smooth muscle-specific proteins smooth-muscle α-actin (0.9±0.2 vs. 1.2±0.3), calponin (0.7±0.1 vs. 1.3±0.1), SM22α (0.5±0.2 vs. 1.3±0.4), and desmin (0.02±0.01 vs. 0.9±0.3) (n=5-6, mean±SEM) all increased upon aligned scaffold-culture, with levels of calponin and desmin increasing significantly. The expression of smooth muscle specific proteins is often reduced/lost upon prolonged cell culture (23, 39). Protein levels from freshly isolated airway tissue were determined separately; with the relative levels of smooth muscle-specific proteins expressed as a ratio to the level of smooth-muscle α-actin. The ratio of smooth muscle α-actin : calponin : SM22α : desmin for airway tissue was 1.0 : 0.9±0.04: 0.7±0.1: 1.2±0.3 , HASM cultured on aligned scaffold was 1.0 : 1.1±0.2 : 1.0±0.2 : 1.0±0.3 , and HASM cultured on 2D TCP was 1.0: 0.7±0.1 : 0.7±0.3 : 0.03±0.02 (n=3-6, mean±SEM).

To investigate HASM cell responses to bronchoconstrictor application, HASM cells cultured either on 2D glass or aligned scaffolds were loaded with the Ca^{2+} sensitive dye Fluo-4-AM and stimulated with the $G\alpha_{q/11}$-agonist BK (100 nM) causing a biphasic increase in $[Ca^{2+}]_i$, with an initial transient increase in Ca^{2+} concentration followed by a reduction to lower steady state Ca^{2+} concentration (7A). HASM cells cultured on glass or the aligned scaffold showed similar levels of peak Ca^{2+} release (7B).

Discussion

Advancements in biomaterial design allow better control to fabricate 3D matrices that are specifically tailored to individual cell-types opposed to the “one rigid 2D substrate fits all” approach offered by TCP. Smooth muscle exists as an aligned population of cells, and this

organization ensures a co-ordinated contractile response. To maintain these characteristics *in vitro*, we electrospun uni-axially orientated fibres to attempt to direct the HASM cell alignment. One previous study has described the alignment of PET fibres by electrospinning onto a rotating mandrel (22). However the rotational velocity employed was much lower than applied here (36 m/min vs. 600 m/min respectively). This large increase in velocity produced thinner nanofibres (0.2 µm vs. 0.7 µm) at similar polymer concentrations (10% vs. 9% *(w/v)*). Comparable micron diameter fibres were produced using a 20% *w/v* polymer solution compared to the 12.5% *w/v* solution (1 µm vs. 1.7 µm fibres). Qualitatively, we demonstrated more consistent alignment of fibres throughout the scaffolds, and greater tensile strength (211 MPa vs. 90 MPa) with respect to aligned nanofibre scaffolds.

When HASM cells were cultured on either a 2D or 3D surface with no orientation reference, only transitory cell alignments were seen over short distances upon contact inhibition. We measured local cell alignment from separate regions of the same sample to investigate cell population alignment over extended distances. The contact guidance provided by fibre orientation ensured good mediation of cell alignment from 3 hours post-seeding, an effect maintained over 14 days. Cells seeded on either aligned scaffold showed consistently good alignment to the fibre orientations (>70% cells within 20^{o} of the scaffold mean fibre angle using either aligned scaffold), though this was still less than cell alignment within *in situ* smooth muscle bundles (>90% cells within 20^{o} of the mean fibre angle). Aligned nanofibres have shown previously to enhance vascular smooth muscle alignment over an immediate time course of 24 hours (51), whilst here we show this effect can be maintained over an extended time period under static conditions. Other studies have achieved similar results with no underlying topological reference through the application of a uni-axially mechanical strain (20), with cells aligning perpendicular to the applied force.

HASM cells cultured in 2D showed clear vinculin localization within defined focal adhesions at the distal ends of the cells, with F-actin and smooth muscle-specific contractile proteins

organised into stress-fibres throughout the cells, an effect most likely caused by the rigidity of the substrate (TCP approximately 2-4 GPa (6)). On the aligned scaffolds, HASM cells showed a reduction in vinculin localization within focal adhesion complexes, and a more even distribution of intra-cellular F-actin, calponin, and SM22α protein expression. Similar reductions in focal adhesions and cytoskeletal organisation have been noted in HASM cells (15, 24), and fibroblasts (1, 27) cultured on 2D surfaces coated with specific extracellular matrix proteins, although HASM cells cultured on these substrates still maintained a flattened cell shape (15, 24). HASM cells cultured in 2D also showed a reduction in elongation compared to those cultured on aligned scaffolds where cells elongated along individual fibres and displayed a more spindle-like morphology than the short, flat, and fat morphology that can occur upon 2D culture. Taken together these data suggest the topography encountered by the smooth muscle may play a dominant role in the cytoskeletal protein organization opposed to the relative rigidity of the substrate, and the cues provided by the aligned fibres ensure HASM cells orientate, and elongate along individual fibres opposed to interacting with multiple fibres as seen when cultured on randomly aligned scaffolds.

Levels of contractile proteins are known to rapidly decrease when HASM cells are passaged upon isolation from fresh tissue (23, 39), with levels of desmin virtually abolished within 7 days post-isolation (23). The culturing of HASM cells on a 3D aligned scaffold was sufficient to significantly increase calponin and desmin protein levels compared to 2D culture, with desmin expression upregulated from negligible levels (2D culture) to consistent expression (3D aligned culture). These expression levels were compared to freshly isolated airway tissue. Relative protein levels, when normalised to smooth muscle α-actin levels, displayed similar expression patterns between airway tissue and 3D-aligned cultured cells; smooth muscle α-actin, calponin and desmin all showing a 1:1 ratio, whilst 3D-aligned cultured cells showed a relative enhancement in calponin expression (1.0 : 0.6). 2D cultured cells showed

a relative reduction in calponin expression and a significant reduction in desmin expression as reported elsewhere (23). Whilst expression patterns are comparable between airway tissue and aligned scaffold cultured cells, the magnitude in protein expression is likely to be underestimated within this study due to the heterogeneous airway cell population used to determine levels of specific smooth muscle proteins within tissue opposed to a homogenous smooth muscle population. Alterations to smooth muscle-specific contractile proteins have also been observed in 3D cultures of HASM cells when cocultured with fibroblasts (48), or fibroblasts and epithelial cells under pulsatile conditions, albeit over an extended time course of 28 days (33). Mechanical strain causes similar alterations to HASM cell contractile protein mRNA and protein levels, including desmin and calponin (2, 20, 45, 55), suggesting similar SMC phenotypic modulations (SMC alignment and contractile protein levels) can be induced through mechanical stimulation, or exposure to a 3D aligned topography. These enhancements in the underlying contractile machinery of the HASM cells could help more accurately model smooth muscle functionality within an *in vitro* setting.

Smooth muscle contraction can be studied using a variety of techniques. Measuring changes in key second-messenger signalling molecules such as $[Ca^{2+}]_i$ have previously been employed in airway- (17) and vascular-smooth muscle (35, 36) contractile profiling. When the bronchoconstrictor BK was applied to HASM cells cultured on 2D or aligned scaffolds, peak Ca^{2+} levels, and Ca^{2+} release profiles were comparable. Given the pronounced alterations in the HASM cellular characteristics and protein levels when cultured on aligned scaffolds compared to 2D culture one may have expected an increase in Ca^{2+} responses. Other studies employing alternative outputs to measure smooth muscle contraction have noted an increase in the comparative shortening of asthmatic smooth muscle compared to healthy smooth muscle (32, 46). A novel multi-cell micro-tissue culture model co-culturing HASM cells with 3T3 fibroblast cells showed alterations in contractile profiles in response to some agonists (such as histamine), but not others (such as KCl) (48).

These suggest underlying differences in Ca^{2+} responses may be uncovered if diseased cells were employed in the present model.

In conclusion, we have developed a fully-aligned nanofibrous scaffold, whose orientation guidance is sufficient to produce fully aligned HASM cell sheets that can be cultured for prolonged periods whilst maintaining a more *in vivo*-like phenotype.

Grants:

This work was funded by the National Centre for the Replacement, Refinement, and Reduction of Animals in Research (NC3Rs) and Asthma UK. Jack Bridge was funded by the EPSRC DTC in Regenerative Medicine.

Figure 1: PET electrospun scaffolds can be manipulated to form aligned nano- and microfibre scaffolds

Polyethylene terephthalate (either 10% or 20% (*w/v*)) was electrospun onto a rotating mandrel (600 metres/min) to produce aligned fibres with diameters in the nano- or micrometre range. Representative SEM images of the 10% (nano) and 20% (micro) scaffolds are shown in 1A and 1B respectively. Intra-scaffold fibre diameter distributions are shown in 1C (n=480 from 3 separate scaffolds), and intra-scaffold fibre alignments are shown in 1D (deviation of individual fibre angle from scaffold's mean fibre angle, n=480 from 3 separate scaffolds).

Table 1: Characteristics of aligned PET scaffolds

The electrospinning parameters used to create PET scaffolds consisting of uni-axially orientated fibres of different diameters are listed in Table 1. The table also shows the average intra-scaffold fibre diameters, the percentage of fibres orientated within +/- 10^{o} mean fibre angle, tensile strength, scaffold thickness, and scaffold porosity as described in material and methods. Data are mean (±SEM) from 3 independently electrospun scaffolds.

Figure 2: HASM cells orientate along scaffold fibres

Haematoxylin and eosin stained immunohistological sections from ASM bundles were used to quantify cell directionality *in situ* (2A). HASM cells ($1.5x10^{5}$) were cultured on glass coverslips, the 10%-, or 20%-aligned scaffolds for 7 or 14 days prior to fixation. Nuclei were visualised by Hoechst staining (blue) and nuclei angles used as reference to cell directionality. Deviation of individual cell nuclei from fibre orientation was determined, and % cell population range plotted. Representative images of HASM nuclei cultured on glass, 10%-, or 20%-aligned scaffolds at day 7 are shown in 2B, 2C, and 2D respectively. 2E shows distribution of cell alignment on all 3 *in vitro* topographies and in ASM bundles. 2F shows % cell population within +/-10^{o} fibre orientation at day 7 and day 14 (mean±SEM, HASM cells cultured on 3 independently electrospun scaffolds). Statistical significance is indicated as *p*=*<0.05, **<0.01, and *p*=****<0.0001 (glass versus), or *p*=≠<0.05, and *p*=≠≠0.01 (bundle versus), one-way ANOVA, Tukeys post-test. Scale bar indicates 40 µm. Arrow indicates orientation of scaffold fibres.

Figure 3: HASM cell morphology is altered when cultured on aligned fibre topography

HASM cells ($1.5x10^5$) were cultured on glass coverslips, 10%-, or 20%-aligned scaffolds for 7 days. Cells were fixed and immunostained for the contractile protein SM22α (red) with nuclei stained with Hoechst (blue). Representative XZ images of HASM cells grown on glass or 10%-aligned scaffolds are shown in 3A&B respectively. Representative 3D opacity images of HASM cells grown on glass or 10%-aligned scaffolds are shown in 3C&D respectively. Representative hematoxylin and eosin stained immunohistological sections from ASM bundles sectioned cross-sectionally and longitudinally are shown in 3E&F respectively. Dashed arrows indicate electrospun-fibre orientation (3B&D). Scale bars represent 20 μm. The heights (*h*) of individual cells were calculated from XZ images through cells. Individual cell's long (*l*) and short (*s*) axis were calculated from XY images, and cell elongation factors determined. Cumulative cell height data is shown in 3G (n=20-82 individual cells grown on 3 independently electrospun scaffolds and 3 separate airway tissue donors). Cumulative cell elongation data is shown in 3H (n=42-73 individual cells grown on 3 independently electrospun scaffolds and 3 separate airway tissue donors). Statistical significance is indicated as *p*=****<0.0001 (glass vs. scaffold), p=≠<0.05 (ASM bundle vs glass), p=≠≠≠≠<0.001 (ASM bundle vs scaffold) one-way ANOVA, Tukeys post-test.

Figure 4: HASM cells show a reduction in intracellular-stress fibres when cultured on aligned fibre topographies

HASM cells ($1.5x10^5$) were cultured on glass coverslips or 10%-aligned scaffolds for 3, 24, or 72 hours prior to fixation. Cells were immunostained for the focal adhesion protein vinculin (red), with F-actin stained with phalloidin (green) and nuclei with Hoechst (blue). Representative images of HASM cultured on glass coverslips for 3-, 24- and 72-hours, and 10%-aligned scaffolds for 3-, 24- or 72-hours are shown in 4A, 4B, 4C, and 4D, 4E, 4F respectively. Scale bar indicates 20 μm. Arrow indicates orientation of scaffold fibres.

Figure 5: Smooth muscle specific protein expression in HASM cells cultured over 14 days on 2D or aligned fibre topography

HASM cells ($1.0x10^5$) were cultured on glass coverslips (5A,C,&E) or 10% aligned scaffolds (5B,D,&,F) for 3, 7, or 14 days prior to fixation. Cells were immunostained for the smooth muscle-specific contractile proteins SM22α (5A&B, red) or calponin (5C&D, green), and the gap-junction protein connexin-43 (5E&F, yellow), with nuclei stained with Hoechst (blue). Scale bar indicates 70 μm. Arrow indicates orientation of scaffold fibres.

Figure 6: Relative HASM cells protein levels are altered when cultured on either 2D or 3D aligned topography

HASM cells ($1.0x10^5$) were cultured on tissue culture plastic (TCP) or 10%-aligned scaffolds for 14 days. Cells were lysed and 20 µg protein loaded for SDS-PAGE separation and immunoblotting. Representative immunoblots for the smooth muscle-specific proteins calponin, SM22α, smooth muscle specific α-actin, desmin, and GAPDH controls are shown in 6A. Cumulative densitometric data showing protein levels normalised to GAPDH protein expression are shown in 6B (data shown are mean(±SEM) n=5-6). Statistical significance is indicated as *p*=*<0.05 and *p*=**0.01 (TCP vs. scaffold) unpaired T-Test.

Figure 7: Primary HASM cells respond to BK when cultured on aligned scaffolds

HASM cells ($1.5x10^5$) were cultured on glass coverslips or aligned scaffolds for 10 days. Cells were loaded with the calcium-sensitive dye Fluo-4 AM and stimulated with BK (100 nM). Representative images showing Ca^{2+} changes, and representative Ca^{2+} traces from HASM cells cultured on glass (black trace) or aligned scaffold (grey trace) and stimulated with BK (100 nM) are shown in 7A. 7B shows cumulative peak Ca^{2+} release from HASM cells stimulated with BK (100 nM) when cultured on glass (black bar) or aligned scaffold (grey bar). Data are mean±SEM (30-60 cells, n=3 separate HASM donors).

1. **Ahmed I, Ponery AS, Nur EKA, Kamal J, Meshel AS, Sheetz MP, Schindler M, and Meiners S.** Morphology, cytoskeletal organization, and myosin dynamics of mouse embryonic fibroblasts cultured on nanofibrillar surfaces. *Mol Cell Biochem* 301: 241-249, 2007.
2. **Ahvaz HH, Soleimani M, Mobasheri H, Bakhshandeh B, Shakhssalim N, Soudi S, Hafizi M, Vasei M, and Dodel M.** Effective combination of hydrostatic pressure and aligned nanofibrous scaffolds on human bladder smooth muscle cells: implication for bladder tissue engineering. *J Mater Sci Mater Med* 23: 2281-2290, 2012.
3. **Beamish JA, He P, Kottke-Marchant K, and Marchant RE.** Molecular regulation of contractile smooth muscle cell phenotype: implications for vascular tissue engineering. *Tissue Eng Part B Rev* 16: 467-491, 2010.
4. **Berair R, Hollins F, and Brightling C.** Airway smooth muscle hypercontractility in asthma. *Journal of allergy* 2013: 185971, 2013.
5. **Billington CK and Penn RB.** Signaling and regulation of G protein-coupled receptors in airway smooth muscle. *Respir Res* 4: 2, 2003.
6. **Butcher DT, Alliston T, and Weaver VM.** A tense situation: forcing tumour progression. *Nat Rev Cancer* 9: 108-122, 2009.
7. **Carroll N, Elliot J, Morton A, and James A.** The structure of large and small airways in nonfatal and fatal asthma. *Am Rev Respir Dis* 147: 405-410, 1993.
8. **Ceresa CC, Knox AJ, and Johnson SR.** Use of a three-dimensional cell culture model to study airway smooth muscle-mast cell interactions in airway remodeling. *Am J Physiol Lung Cell Mol Physiol* 296: L1059-1066, 2009.
9. **Chew SY, Mi R, Hoke A, and Leong KW.** The effect of the alignment of electrospun fibrous scaffolds on Schwann cell maturation. *Biomaterials* 29: 653-661, 2008.
10. **Cockcroft DW.** Direct challenge tests: Airway hyperresponsiveness in asthma: its measurement and clinical significance. *Chest* 138: 18S-24S, 2010.
11. **Corey JM, Gertz CC, Wang BS, Birrell LK, Johnson SL, Martin DC, and Feldman EL.** The design of electrospun PLLA nanofiber scaffolds compatible with serum-free growth of primary motor and sensory neurons. *Acta Biomater* 4: 863-875, 2008.
12. **Crouch AS, Miller D, Luebke KJ, and Hu W.** Correlation of anisotropic cell behaviors with topographic aspect ratio. *Biomaterials* 30: 1560-1567, 2009.
13. **Cukierman E, Pankov R, Stevens DR, and Yamada KM.** Taking cell-matrix adhesions to the third dimension. *Science* 294: 1708-1712, 2001.
14. **Cukierman E, Pankov R, and Yamada KM.** Cell interactions with three-dimensional matrices. *Curr Opin Cell Biol* 14: 633-639, 2002.
15. **D'Antoni ML, Risse PA, Ferraro P, Martin JG, and Ludwig MS.** Effects of decorin and biglycan on human airway smooth muscle cell adhesion. *Matrix Biol* 31: 101-112, 2012.
16. **Dalton PD, Vaquette C, Farrugia BL, Dargaville TR, Brown TD, and Hutmacher DW.** Electrospinning and additive manufacturing: converging technologies. *Biomater Sci* 1: 171-185, 2012.
17. **Deshpande DA, Dogan S, Walseth TF, Miller SM, Amrani Y, Panettieri RA, and Kannan MS.** Modulation of calcium signaling by interleukin-13 in human airway smooth muscle: role of CD38/cyclic adenosine diphosphate ribose pathway. *Am J Respir Cell Mol Biol* 31: 36-42, 2004.
18. **Dunnill MS, Massarella GR, and Anderson JA.** A comparison of the quantitative anatomy of the bronchi in normal subjects, in status asthmaticus, in chronic bronchitis, and in emphysema. *Thorax* 24: 176-179, 1969.
19. **Elliott JT, Woodward JT, Langenbach KJ, Tona A, Jones PL, and Plant AL.** Vascular smooth muscle cell response on thin films of collagen. *Matrix Biol* 24: 489-502, 2005.

20. **Fairbank NJ, Connolly SC, Mackinnon JD, Wehry K, Deng L, and Maksym GN.** Airway smooth muscle cell tone amplifies contractile function in the presence of chronic cyclic strain. *Am J Physiol Lung Cell Mol Physiol* 295: L479-488, 2008.
21. **Farmer SG, Ensor JE, and Burch RM.** Evidence that cultured airway smooth muscle cells contain bradykinin B2 and B3 receptors. *Am J Respir Cell Mol Biol* 4: 273-277, 1991.
22. **Hadjizadeh A, Ajji A, and Bureau MN.** Nano/micro electro-spun polyethylene terephthalate fibrous mat preparation and characterization. *J Mech Behav Biomed Mater* 4: 340-351, 2011.
23. **Halayko AJ, Salari H, Ma X, and Stephens NL.** Markers of airway smooth muscle cell phenotype. *Am J Physiol* 270: L1040-1051, 1996.
24. **Hirst SJ, Twort CH, and Lee TH.** Differential effects of extracellular matrix proteins on human airway smooth muscle cell proliferation and phenotype. *Am J Respir Cell Mol Biol* 23: 335-344, 2000.
25. **Jeffery PK.** Remodeling in asthma and chronic obstructive lung disease. *Am J Respir Crit Care Med* 164: S28-38, 2001.
26. **Johansson F, Carlberg P, Danielsen N, Montelius L, and Kanje M.** Axonal outgrowth on nano-imprinted patterns. *Biomaterials* 27: 1251-1258, 2006.
27. **Kapoor A and Sen S.** Synergistic modulation of cellular contractility by mixed extracellular matrices. *Int J Cell Biol* 2012: 471591, 2012.
28. **Kaur D, Saunders R, Berger P, Siddiqui S, Woodman L, Wardlaw A, Bradding P, and Brightling CE.** Airway smooth muscle and mast cell-derived CC chemokine ligand 19 mediate airway smooth muscle migration in asthma. *Am J Respir Crit Care Med* 174: 1179-1188, 2006.
29. **Kim DH, Provenzano PP, Smith CL, and Levchenko A.** Matrix nanotopography as a regulator of cell function. *J Cell Biol* 197: 351-360, 2012.
30. **Lambert RK, Wiggs BR, Kuwano K, Hogg JC, and Pare PD.** Functional significance of increased airway smooth muscle in asthma and COPD. *J Appl Physiol* 74: 2771-2781, 1993.
31. **Marsh KA and Hill SJ.** Characteristics of the bradykinin-induced changes in intracellular calcium ion concentration of single bovine tracheal smooth muscle cells. *Br J Pharmacol* 110: 29-35, 1993.
32. **Matsumoto H, Moir LM, Oliver BG, Burgess JK, Roth M, Black JL, and McParland BE.** Comparison of gel contraction mediated by airway smooth muscle cells from patients with and without asthma. *Thorax* 62: 848-854, 2007.
33. **Miller C, George S, and Niklason L.** Developing a tissue-engineered model of the human bronchiole. *J Tissue Eng Regen Med* 4: 619-627, 2010.
34. **Moreno MJ, Ajji A, Mohebbi-Kalhori D, Rukhlova M, Hadjizadeh A, and Bureau MN.** Development of a compliant and cytocompatible micro-fibrous polyethylene terephthalate vascular scaffold. *J Biomed Mater Res B Appl Biomater* 97: 201-214, 2011.
35. **Morris GE, Nelson CP, Everitt D, Brighton PJ, Standen NB, Challiss RA, and Willets JM.** G protein-coupled receptor kinase 2 and arrestin2 regulate arterial smooth muscle P2Y-purinoceptor signalling. *Cardiovasc Res* 89: 193-203, 2011.
36. **Morris GE, Nelson CP, Standen NB, Challiss RA, and Willets JM.** Endothelin signalling in arterial smooth muscle is tightly regulated by G protein-coupled receptor kinase 2. *Cardiovasc Res* 85: 424-433, 2010.
37. **Murray-Dunning C, McArthur SL, Sun T, McKean R, Ryan AJ, and Haycock JW.** Three-dimensional alignment of schwann cells using hydrolysable microfiber scaffolds: strategies for peripheral nerve repair. *Methods Mol Biol* 695: 155-166, 2011.
38. **Paik I, Scurr DJ, Morris B, Hall G, Denning C, Alexander MR, Shakesheff KM, and Dixon JE.** Rapid micropatterning of cell lines and human pluripotent stem cells on elastomeric membranes. *Biotechnol Bioeng* 109: 2630-2641, 2012.
39. **Panettieri RA, Murray RK, DePalo LR, Yadvish PA, and Kotlikoff MI.** A human airway smooth muscle cell line that retains physiological responsiveness. *Am J Physiol* 256: C329-335, 1989.

40. **Parrag IC, Zandstra PW, and Woodhouse KA.** Fiber alignment and coculture with fibroblasts improves the differentiated phenotype of murine embryonic stem cell-derived cardiomyocytes for cardiac tissue engineering. *Biotechnol Bioeng* 109: 813-822, 2012.
41. **Schnell E, Klinkhammer K, Balzer S, Brook G, Klee D, Dalton P, and Mey J.** Guidance of glial cell migration and axonal growth on electrospun nanofibers of poly-epsilon-caprolactone and a collagen/poly-epsilon-caprolactone blend. *Biomaterials* 28: 3012-3025, 2007.
42. **Shang S, Yang F, Cheng X, Walboomers XF, and Jansen JA.** The effect of electrospun fibre alignment on the behaviour of rat periodontal ligament cells. *Eur Cell Mater* 19: 180-192, 2010.
43. **Sill TJ and von Recum HA.** Electrospinning: applications in drug delivery and tissue engineering. *Biomaterials* 29: 1989-2006, 2008.
44. **Skloot G, Permutt S, and Togias A.** Airway hyperresponsiveness in asthma: a problem of limited smooth muscle relaxation with inspiration. *J Clin Invest* 96: 2393-2403, 1995.
45. **Smith PG, Moreno R, and Ikebe M.** Strain increases airway smooth muscle contractile and cytoskeletal proteins in vitro. *Am J Physiol* 272: L20-27, 1997.
46. **Sutcliffe A, Hollins F, Gomez E, Saunders R, Doe C, Cooke M, Challiss RA, and Brightling CE.** Increased nicotinamide adenine dinucleotide phosphate oxidase 4 expression mediates intrinsic airway smooth muscle hypercontractility in asthma. *Am J Respir Crit Care Med* 185: 267-274, 2012.
47. **Teo WE and Ramakrishna S.** A review on electrospinning design and nanofibre assemblies. *Nanotechnology* 17: R89-R106, 2006.
48. **West AR, Zaman N, Cole DJ, Walker MJ, Legant WR, Boudou T, Chen CS, Favreau JT, Gaudette GR, Cowley EA, and Maksym GN.** Development and characterization of a 3D multicell microtissue culture model of airway smooth muscle. *Am J Physiol Lung Cell Mol Physiol* 304: L4-16, 2013.
49. **Wozniak MA, Modzelewska K, Kwong L, and Keely PJ.** Focal adhesion regulation of cell behavior. *Biochim Biophys Acta* 1692: 103-119, 2004.
50. **Wright D, Sharma P, Ryu MH, Risse PA, Ngo M, Maarsingh H, Koziol-White C, Jha A, Halayko AJ, and West AR.** Models to study airway smooth muscle contraction in vivo, ex vivo and in vitro: Implications in understanding asthma. *Pulm Pharmacol Ther*, 2012.
51. **Xu CY, Inai R, Kotaki M, and Ramakrishna S.** Aligned biodegradable nanofibrous structure: a potential scaffold for blood vessel engineering. *Biomaterials* 25: 877-886, 2004.
52. **Yamada KM and Cukierman E.** Modeling tissue morphogenesis and cancer in 3D. *Cell* 130: 601-610, 2007.
53. **Yang F, Murugan R, Wang S, and Ramakrishna S.** Electrospinning of nano/micro scale poly(L-lactic acid) aligned fibers and their potential in neural tissue engineering. *Biomaterials* 26: 2603-2610, 2005.
54. **Yim EK, Reano RM, Pang SW, Yee AF, Chen CS, and Leong KW.** Nanopattern-induced changes in morphology and motility of smooth muscle cells. *Biomaterials* 26: 5405-5413, 2005.
55. **Zhang X, Wang X, Keshav V, Wang X, Johanas JT, Leisk GG, and Kaplan DL.** Dynamic culture conditions to generate silk-based tissue-engineered vascular grafts. *Biomaterials* 30: 3213-3223, 2009.

653 Figure 1

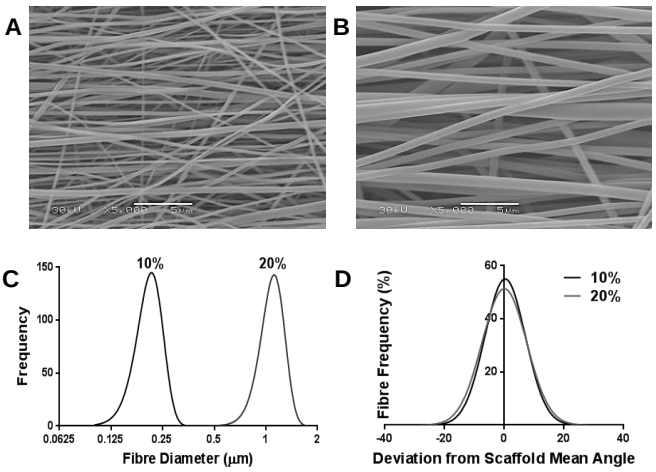

654

655 Figure 2

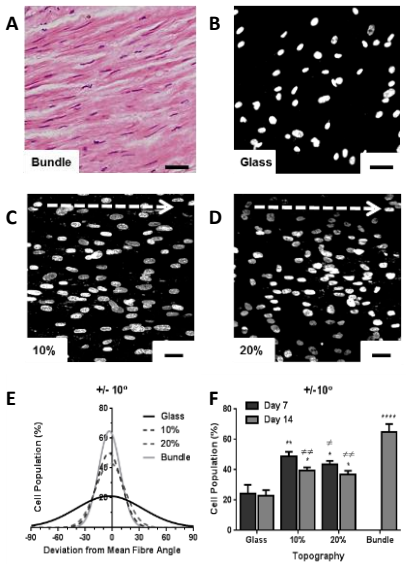

656

657 Figure 3

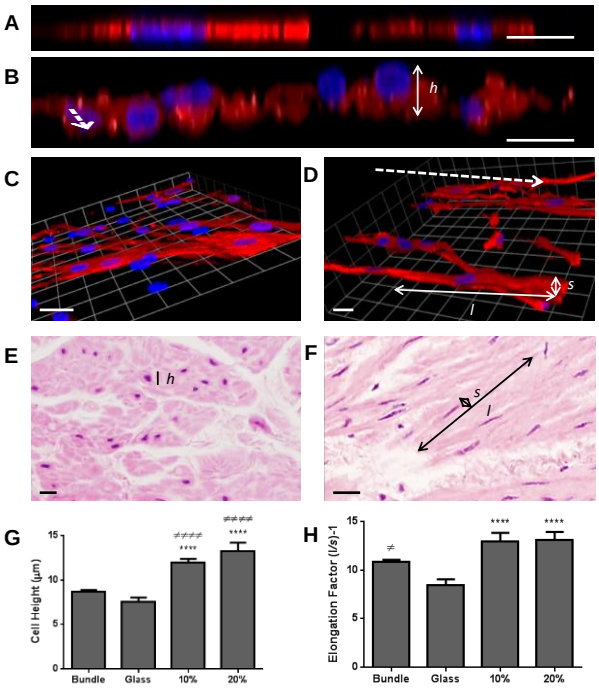

658

659 Figure 4

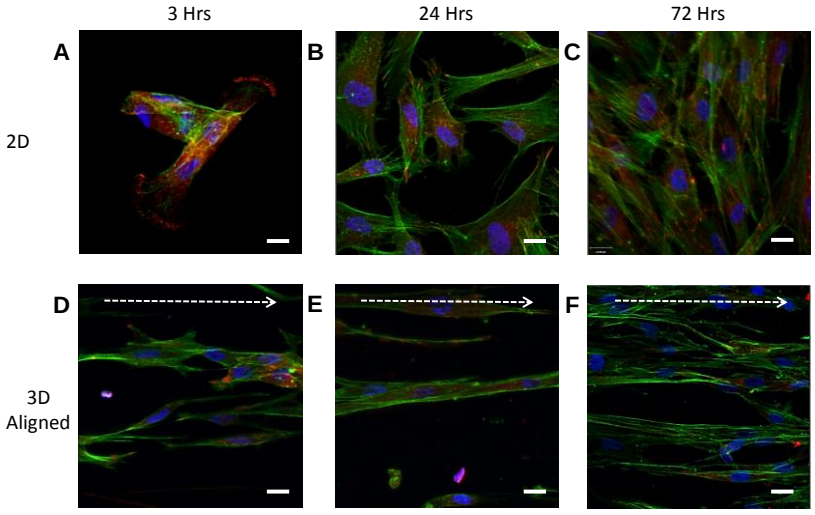

660

661 Figure 5

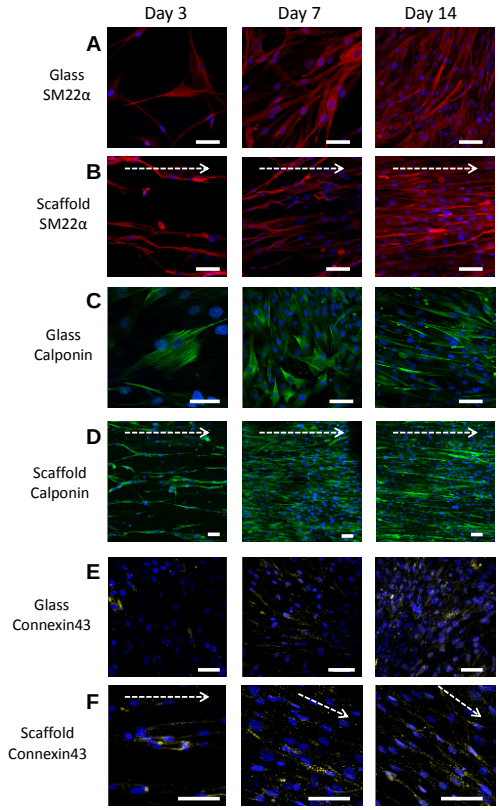

662

663 Figure 6

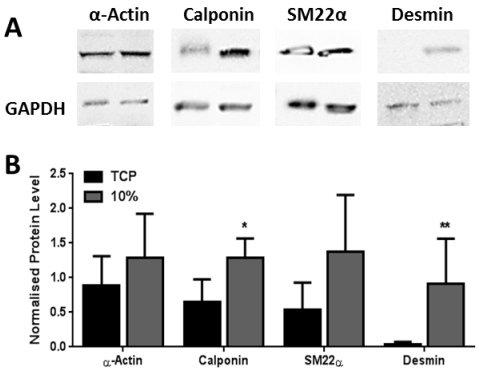

664

665 Figure 7

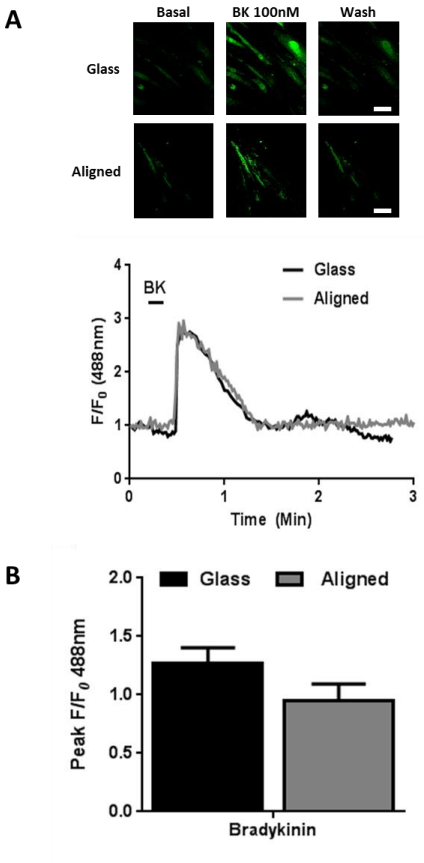

666